The Impact of Temperature on Thermal Fluctuations in Magnetic Nanoparticle Systems

K. Everaert,[1,2] B. Van Waeyenberge,[1] F. Wiekhorst,[2] and J. Leliaert[1]
[1)] *Department of Solid State Sciences, Ghent University, 9000 Ghent, Belgium*
[2)] *Physikalisch-Technische Bundesanstalt, 10587 Berlin, Germany*

(*Electronic mail: katrijn.everaert@ugent.be / katrijn.everaert@ptb.de)

(Dated: 29 April 2023)

We investigate the effect of temperature on the thermal magnetic noise signal of magnetic nanoparticle (MNP) systems as models for non-interacting macrospins. An analytical expression for the amplitude of the fluctuations in a magnetic field is derived for the Brownian and the Néel fluctuation mechanisms, and compared with numerical results at different temperatures. To experimentally validate our findings, magnetic noise spectra of two commercially available polydisperse MNP systems (Ferucarbotran and Perimag) were measured at different, biomedically relevant temperatures. A distinctive effect of temperature on the power spectral noise densities is measurable already for 5 K temperature differences and, within the bandwidth of the experiment, higher noise amplitudes are found for lower temperatures. However, a crossing of the spectra at higher frequencies is revealed in simulations, so that the total fluctuation amplitude is conserved. These findings contribute to a profound understanding of temperature influences on MNP fluctuation and relaxation mechanisms.

Thermal noise in nanomagnetic structures manifests itself when the thermal energy becomes comparable to the magnetic anisotropy barrier[1]. In the context of data storage, magnetic thermal fluctuations are often seen in a bad light, as they induce information loss[2]. However, the thermal fluctuations in magnetic micro- and nanostructures can also be used to our advantage. e.g. by using the switching of the magnetic domains as input for a random variable generator for probabilistic computing[3?,4]. The study of the thermal magnetic noise itself has the advantage that the experiments can be performed at thermal equilibrium, without the need of an external perturbation. As a consequence, clean and unbiased information about the magnetization dynamics of the involved components are obtained[5–7].

In this letter, fluctuations in magnetic nanoparticle (MNP) systems are investigated[8]. We consider MNPs that are single domain particles and can be represented by single macrospins. The thermal reorientations of the moments in the anisotropy energy landscape are called Néel fluctuations. MNPs are often suspended in a fluid where they freely move and rotate. This gives rise to an additional fluctuation mechanism: the commonly known Brownian fluctuations[9]. Thanks to their size, their functionalizable surface, and their magnetic properties, MNPs are used in many different biomedical applications[10–12]. To this end, they are being exposed to and operating at a wide range of temperatures, which strongly influences their magnetic properties and dynamic response.

As described by the Fluctuation Dissipation Theorem[13], thermal fluctuations drive the relaxation of the moments towards an equilibrium state, and this can be related to the dissipated heat under the application of an AC field by the imaginary component of the susceptibility[14]. Understanding the fluctuation dynamics and its dependence on temperature thus improves the applicability of MNPs for biomedical purposes.

MNP ensembles are often said to be in a *superparamagnetic* state, meaning that the magnetic moments of their ferromagnetic single-domain cores are thermally switching at the timescale of observation. At lower temperatures, the thermal energy becomes insufficient so that the magnetic moments can no longer overcome the energy barrier set by the anisotropy at experimental timescales. As a consequence, the moments are thermally blocked, and the particle ensemble is said to be ferromagnetic. This is the principle behind zero-field cooled (ZFC) and field cooled (FC) measurements, which serve to determine the anisotropy energy distribution of a sample[15]. A blocking temperature T_B is often defined for a nanoparticle system, which is the temperature where the anisotropy energy equals the thermal energy. Note however that the superparamagnetic-ferromagnetic transition is not a real physical phase transition. Since the system is still ergodic beneath T_B, there is still a finite chance for the magnetization to reach each state of the phase space, and therefore to eventually flip against the direction preferred by the anisotropy. At infinite observation timescales, this flip will take place. In a statistical context, all particles are assumed to be superparamagnetic below the Curie temperature T_C of their core material.

Apart from the fluctuation mechanisms themselves, intrinsic material properties such as the anisotropy and the amplitude of the magnetic moment might be temperature dependent as well[16]. We take those parameters constant and present a framework of the temperature dependence of the thermal noise of a non-interacting macrospin ensemble. Our findings are compared with numerical and experimental results.

The origin of the fluctuations in the magnetic signal of a MNP sample lies in the reorientation of the magnetic moments of the MNP. Thermally driven, the magnetic moment $\vec{m}$ of a MNP rotates on a sphere with radius $\|\vec{m}\|$. The couple of spherical angles ($\theta \in [0, 2\pi[, \psi \in [0, \pi[$) defines the phase space Ω of the moment. We call the magnetic moment $\vec{m}$ the primary stochastic variable.

Rotations of $\vec{m}$ can directly be measured in magneto-optical experiments[17,18]. However, magnetometers are more common to investigate MNP ensembles in a suspension. They measure the magnetic field $\vec{B}$ generated by the MNPs at a certain lo-

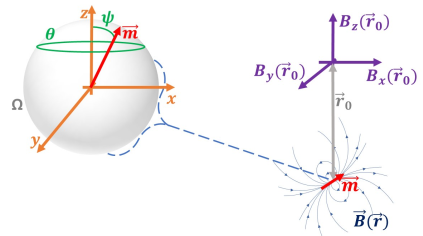

FIG. 1. Scheme of the involved stochastic variables. The magnetic moment $\vec{m}$ of a MNP is the primary stochastic variable which takes random orientation from a phase space Ω described by a sphere with radius $\|\vec{m}\|$. The fluctuations in $\vec{m}$ are measured by a magnetometer at distance $\vec{r}_o$ form the MNP. The magnetic field $\vec{B}$ is called the secondary stochastic variable.

cation $\vec{r}_0$. $\vec{B}$ is the secondary stochastic variable which can be written as a function of the primary stochastic variable. A dipolar field is used to describe the field generated by a magnetic moment $\vec{m}$ at distance r:

$$\vec{B}(\vec{r}) = \frac{\mu_0}{4\pi}\left(\frac{3\vec{r}(\vec{m}\cdot\vec{r})}{\|\vec{r}\|^5} - \frac{\vec{m}}{\|\vec{r}\|^3}\right) \tag{1}$$

The expected values and central moments of the secondary variable can now be calculated by integrating over the distribution of the primary stochastic variable $\vec{m}$. This distribution depends on the mechanism which drives the fluctuations, and a differentiation is necessary. In the following, we present the theoretical calculation of the central moments of the secondary stochastic variable $\vec{B}$ for the two fluctuation mechanisms. Note that, depending on the type of magnetic sensor, only certain components of the magnetic field vector can be measured experimentally, e.g. SQUID magnetometers only measure the flux in the direction perpendicular to the pickup coil. We therefore refer generally to the value of interest with $\mathbb{B} = \{\vec{B}, B_x, B_y, B_z\}$. Details on the calculations can be found in the supplementary material. Spherical coordinates are used to describe the phase space Ω of $\vec{m}$, with azimuthal angle θ and polar angle ψ. Without loss of generality, the sensing vector $\vec{r}$ is chosen along the z direction of the coordinate system at a distance d from the magnetic moment: $\vec{r} = (0,0,d)$.

Firstly, we consider Brownian fluctuations that are induced by the physical rotation of particles suspended in a fluid[9]. In the absence of an external magnetic field, the moments have no preferred direction in phase space. The probability density function (PDF) of the magnetic moments is thus uniform for Brownian rotations. The PDF - shown on Fig. 2 - is written as:

$$\mathrm{PDF}^{Br}_{\vec{m}}(\theta,\psi) = \frac{1}{4\pi}\sin\psi. \tag{2}$$

The first central moment of the secondary stochastic variable $\vec{B}$ is calculated by weighting the expression for the dipole field Eq. (1) by the PDF of the primary stochastic variable $\vec{m}$.

$$\langle\mathbb{B}(\vec{r})\rangle = \int_0^{2\pi}\int_0^{\pi}\mathrm{PDF}^{Br}_{\vec{m}}(\theta,\psi)\mathbb{B}(\vec{r})d\psi d\theta = 0 \tag{3}$$

Not surprisingly, the first central moment, i.e. the average of the fluctuations in the magnetic field, is zero. The second central moment, i.e. the variance, is calculated in a similar way:

$$\langle\mathbb{B}^2(\vec{r})\rangle \begin{cases} \langle B_i^2(\vec{r})\rangle = \int_0^{2\pi}\int_0^{\pi}\mathrm{PDF}^{Br}_{\vec{m}}(\theta,\psi)B_i^2(\vec{r})d\psi d\theta = \frac{1}{3}\left(\frac{\mu_0 m}{4\pi d^3}\right)^2 \text{ with } i = x,y \\ \langle B_z^2(\vec{r})\rangle = \int_0^{2\pi}\int_0^{\pi}\mathrm{PDF}^{Br}_{\vec{m}}(\theta,\psi)B_x^2(\vec{r})d\psi d\theta = \frac{4}{3}\left(\frac{\mu_0 m}{4\pi d^3}\right)^2 \\ \langle\vec{B}^2(\vec{r})\rangle = \int_0^{2\pi}\int_0^{\pi}\mathrm{PDF}^{Br}_{\vec{m}}(\theta,\psi)\vec{B}^2(\vec{r})d\psi d\theta = 2\left(\frac{\mu_0 m}{4\pi d^3}\right)^2 \end{cases} \tag{4}$$

The variance of the fluctuations in the direction of sensing is 4 times larger than the perpendicular components. Higher central moments can be calculated in a similar way.

The lateral movement of a MNP due to Brownian translational motion also contributes to the fluctuations in the magnetic field, but can in many cases be neglected compared to the MNP rotation. The displacement is described by a normal distribution with a variance $\sigma^2 = 2Dt$:

$$\mathrm{PDF}^{Br}_{\vec{r}}(\vec{r},t) = \frac{\exp\left(-\frac{x^2+y^2+z^2}{4\pi Dt}\right)}{(4\pi^2 Dt)^{3/2}}. \tag{5}$$

Here, t is the time of the measurement and D the diffusion coefficient given by

$$D = \frac{k_B T}{3\pi\eta d_h} \tag{6}$$

We will discuss the contribution of Brownian translation after introducing the timescales of the fluctuation mechanisms.

Secondly, Néel fluctuations are fluctuations of the magnetic moment within the crystal structure of the MNP[1]. Assuming uniaxial magnetocrystalline or shape anisotropy, it requires the magnetic moments to overcome an anisotropy barrier with associated energy $E = KV\sin^2(\psi)$ to switch direction. We choose the anisotropy axis to be oriented along the z axis, which makes ψ the angle between the magnetic moment and the anisotropy axis. Thermal energy drives deviations from

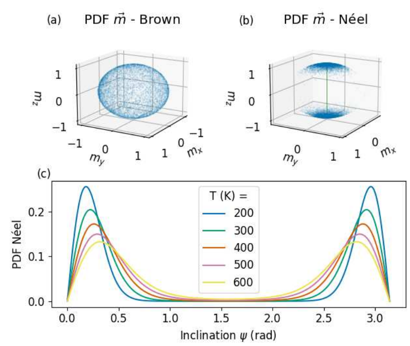

FIG. 2. Probability distribution of primary stochastic variable $\vec{m}$ for the two fluctuation mechanisms. (a) 10000 random orientations of $\vec{m}$ chosen following the PDF of Brownian rotation Eq. 2. The distribution is uniform over the full phase space and independent of temperature. (b) 10000 random orientations of $\vec{m}$ chosen following the PDF of Néel fluctuations Eq. 7 at T=300 K. The other particle properties are described in the supplementary material. A preferred direction is visible along anisotropy axis, shown in green. (c) The PDF for Néel fluctuations at different temperatures as function of the inclination ψ. Note that the PSD goes to 0 for $\psi = \{0, \pi\}$ due to the density of states in the spherical parametrisation.

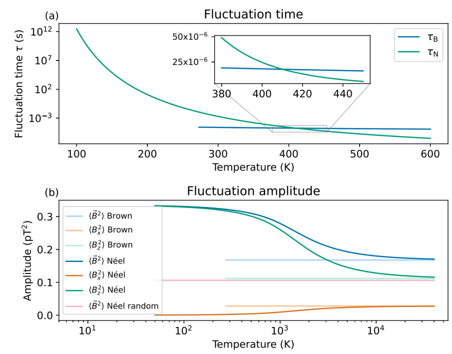

FIG. 3. Dependence of fluctuation time and amplitude on temperature. (a) Brownian and Néel fluctuation times as given by Eq. (9) and Eq. (10), with parameters η =1mPas, $d_c = 24$ nm, $d_h = 30$ nm, $K = 10$ kJ/m^3, $\tau_0 = 4\text{x}10^{-9}$ s. (b) Brownian fluctuation amplitudes as given by Eq. (4) and Néel fluctuation amplitudes as given Eq. (8) for the case of parallel sensing and anisotropy axes. Note that for the limiting case of $\lim T \to \infty$, $\alpha = 0$ so that Néel fluctuation amplitudes coincide with Brownian fluctuation amplitudes. If the anisotropy axes are distributed randomly, the fluctuation amplitude is independent of temperature.

the preferred anisotropic direction with a probability density function described by Maxwell-Boltzmann statistics:

$$\text{PDF}_{\vec{m}}^{Ne}(\theta, \psi) = \xi \sin(\psi) \exp(-\alpha \sin^2 \psi) \quad (7)$$

with $\xi = \frac{\sqrt{\alpha}}{2\pi^{\frac{3}{2}} \exp(-\alpha)\text{Erfi}(\sqrt{\alpha})}$ the normalization factor, $\alpha = \frac{KV}{k_B T}$ and Erfi the imaginary error function. With increasing temperature, the orientations of the magnetic moments deviate more from the anisotropy axis, as shown on Fig. 2 c.
The central moments of the secondary stochastic variable cannot be solved analytically as in the case of Brownian rotations. The expressions can be calculated numerically, as shown in Fig. 3:

$$\langle \mathbb{B}^2(\vec{r}) \rangle = \int_0^{2\pi} \int_0^{\pi} \text{PDF}_{\vec{m}}^{Ne}(\theta, \psi) \mathbb{B}^2(\vec{r}) d\psi d\theta \quad (8)$$

Including now the notion of time, the stochastic variables $\vec{m}$ and $B(\vec{m})$ become time dependent stochastic processes $\vec{m}(t)$ and $B(\vec{m}, t)$. These are considered to be static and ergodic, so that time averages equal ensemble averages. The magnetic moments evolve within the phase space Ω, leading to fluctuations of the magnetic signal at certain timescales and with certain amplitudes. We further describe the influence of temperature on the fluctuation amplitude and the fluctuation timescale, both for single particles and polydisperse particle ensembles.

The two fluctuation mechanisms each have a characteristic timescales. The magnetic moment of a particle under influence of Brownian motion rotates at timescales[19]

$$\tau_B = \frac{3\eta V_h}{k_B T} \quad (9)$$

with V_h the hydrodynamic volume, k_B the Boltzmann constant, T the temperature, and η the viscosity of the fluid. The average lateral displacement of the MNP on this timescale is given by the standard deviation of the PDF of Brownian translational motion in Eq. (5): $\sigma = \sqrt{2D\tau_B} = \frac{d_h}{\sqrt{3}}$. In experiments where this displacement has a significant contribution to the signal fluctuations compared to that of the rotation, Brownian translational motion should be taken into account. However, for macroscopic experimental geometries, this contribution can be neglected.

The timescales of Néel fluctuations are described by

$$\tau_N = \tau_0 \exp\left(\frac{KV_c}{k_B T}\right) \quad (10)$$

where K is the anisotropy constant, V_c the core volume of the particle, and τ_0 a attempt time, typically in the order of 10^{-8} - 10^{-12} s. A combined fluctuation time is then defined as

$$\tau_{\text{eff}} = \frac{\tau_N \tau_B}{\tau_N + \tau_B} \quad (11)$$

where often, only one mechanism - the faster one - is dominant.

Eq. (9) and (10) are plotted as a function of temperature in Fig. 3a. A strong dependence of the Néel fluctuation time and a small dependence of the Brownian fluctuation time is visible. A crossing occurs around 410 K for the parameters considered here.

The amplitude of the fluctuations depends on what is the observed variable, and thus on the measurement method and the geometry of the experiment. It is defined by how much the signal deviates from its mean value and is thus quantified by the variance or the standard deviation. In this work, we use the variance as measure for the amplitude of the fluctuations, which is sometimes called noise power.

The amplitude of Brownian fluctuations is independent of temperature, as described by Eq. (4) and shown on Fig. 3b. Upon increase of the temperature, all points on Ω are reached with equal probability, and the amplitude of the fluctuations along the sensing direction is 4 times higher than that perpendicular to it. In the case of Néel fluctuation however, the amplitude strongly depends on temperature. Fig. 3b shows the situation where the anisotropy axis lies parallel to sensing axis. The dependence of the component along this axis is counter intuitive, as the fluctuation amplitude decreases with increasing temperature. Taking a look at the PDF displayed on Fig. 2 explains this behavior. The moments deviate further from the anisotropy axis at higher temperatures, and the variance of the moment component projected on this axis therefore decreases. The fluctuations in the moments perpendicular to this axis increase in amplitude with increasing temperature. In the limit $\lim_{T\to\infty}$ or $\lim_{\alpha\to 0}$, there is effectively no anisotropy barrier anymore and the Néel amplitudes match the Brownian amplitudes. Fig. 3b also shows the amplitude of the fluctuations in the magnetic field for randomly oriented anisotropy axes. In this case, the fluctuation amplitude is smaller, and independent of temperature.

The autocorrelation function of the magnetic signal decays exponentially

$$G^{\mathbb{B}}(t) = \langle \mathbb{B}(0)\mathbb{B}(t)\rangle = \langle \mathbb{B}^2\rangle \exp(-|t|/\tau). \tag{12}$$

and the Power Spectral Density (PSD) is obtained from the Wiener-Khintchine theorem as the Fourier transform of the autocorrelation function[20,21]:

$$S^{\mathbb{B}}(f) = \langle \mathbb{B}^2\rangle \frac{(2\tau)^{-1}}{(\pi f)^2 + (2\tau)^{-2}} \tag{13}$$

The integration of the PSD over bandwidth Δf gives the noise power in this frequency range.

Fig. 4 shows the PSDs for a single MNP fluctuating under the Brownian (a-b) or Néel (c-f) rotation mechanism at two different temperatures[22]. The analytic expression Eq. (13) is plotted with the PSD of the simulated signals. The amplitude $\langle \mathbb{B}^2\rangle$ of the analytical expression is calculated following Eq. (4) and (8), and the fluctuation times τ from Eq. (9) and Eq. (10) are employed, with $\tau_0 = 6.5\text{x}10^{-11}$ s.

The signals from Brownian fluctuations are plotted for T=275 K and T=340 K in panels 4 (a) and (b). A good agreement between the simulation and the analytical expression is found. A limited effect of temperature is visible, as the fluctuation time depends only linearly on T (Eq. (9)). The PSD for

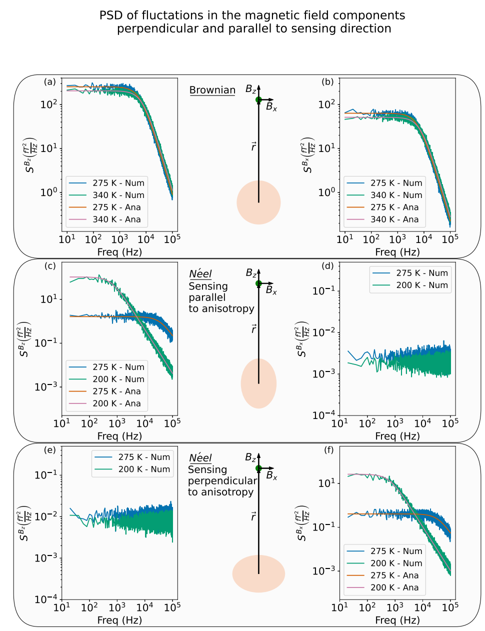

FIG. 4. Analytical and numerical PSDs of Brownian and Néel fluctuations of a single MNP in the magnetic field components perpendicular (a,c,e) and parallel (b,d,f) to the sensing direction at different temperatures. The analytical expressions from Eq. (4) and (13) are denoted Ana, and the PSD form the numerical signals are denoted Num. The direction of the anisotropy axis is visualized by the long axis of the ellipse.

T=275 K has higher power at lower frequencies, but the PSDs cross each other at about $f = 5\text{x}10^3$ Hz and the total amplitude (i.e. the area under the curves) is independent of temperature as described by Eq. (4). The amplitude of the fluctuations along the sensing direction in panel 4 (a) is 4 times larger than those perpendicular to the sensing direction in panel 4 (b).

As the dependence of Néel fluctuations on temperature depends on the geometry of the measurement, two different scenarios are given in Fig. 4 for T=200 K and T=275 K. The PSD describing the switching of the moment over the anisotropy barrier (the inter-potential-well fluctuations[23]) is found in the magnetic field component along the anisotropy axis (panels 4 (c) and (f)). The component perpendicular to the anisotropy axis senses the fluctuations within the potential well (the intra-potential-well fluctuations) which PSD is shown on panels 4 (d) and (e). They typically occur at much smaller timescales[23,24] and only the white part of this noise is captured in the considered frequency range. Large differences in the PSDs are found for the inter-potential-well fluctuations at different temperatures, due to the exponential dependence of the fluctuation time on temperature (Eq. (10)). Additionally, the amplitude of the fluctuations (i.e. the area under the PSD) along the anisotropy axis decreases for increasing temperature as described by Eq. (8); a counter intuitive phenomenon which is recovered in the numerical results. For randomly oriented anisotropy axes, the dependence in the amplitude of Néel fluctuations on temperature cancels, i.e. the dependence of the area under the PSD. However, there will still be a strong dependence of the fluctuation timescale on temperature. This affects the width of the PSD, and consequently power density at a fixed frequency.

A more realistic scenario of a polydisperse MNP ensemble is now considered, as MNP samples used in biomedical studies in reality always display a non-zero size distribution. Their diameters are typically described by a lognormal distribution and the volumes V_h and V_c are distributed along distribution $P(V_h)$ and $P(V_c)$. The PSD of the full ensemble can then be written as a superposition of the individual fluctuators:

$$S^{\mathbb{B}}_{\text{poly}}(f) = \int_0^\infty P(\tau) S^{\mathbb{B}}_\tau(f) d\tau_{\text{eff}} \quad (14)$$

$$= \int_0^{V_c} \int_0^\infty P(V_h) P(V_c) S^{\mathbb{B}}_{V_c,V_h}(f) dV_c dV_h \quad (15)$$

The same properties of single particles apply to particle ensembles, though weighted over the size distributions.

Thermal fluctuations in the magnetic signal of two commercially available MNP systems were measured at different biomedically relevant temperatures. 200 μl of Perimag (Micromod Partikeltechnologie, Rostock, Germany) and Ferucarbotran (FCT, Meito Sanyo Co., Nagoya, Japan) solutions with an iron concentration of 138 and 445 mmol/l resp. were placed inside a superconducting shield[25] and the magnetic signal was recorded for 13 min. with a SQUID magnetometer. Due to their large core sizes, both MNP systems fluctuate by the Brownian rotational mechanism. The effect of the Brownian translation in the macroscopic geometry of the experiment was found to be 5 orders of magnitude smaller that of the rotation. Temperature was varied by applying a stable airflow through the sample space, and a deviation smaller than 0.5 K from the aimed temperature at the sample position was assured by tracking temperature with a fiber optic probe thermometer during measurement. The experimental PSDs of both MNP systems are shown in Fig. 5 (a) and (d). A lognormal size distribution is fitted to the PSDs at the lowest temperatures (24C (297.15 K) and 25C (298.15 K) for FCT and Perimag respectively) which is subsequently used as input for the comparing simulations. More details on this can be found in the supplementary material. Fig. 5 (b) and (e) show the resulting PSDs from the simulations.

A clear influence of temperature on the thermal fluctuations in the experiments is visible in Fig. 5 (a) and (d). FCT shows a cuttof regime at $10^2 - 10^3$ Hz beneath which the PSD is flat and above which the PSD falls of with $1/f^2$. On the contrary, due to Perimags large particles and broad size distribution, no clear cutoff range is visible and its PSD falls off gradually. Altough the iron concentration of Perimag is about 1/3 of the concentration used for FCT, the signal of Perimag is a factor of 10 higher than that of FCT. This is explained by the fact that the signal not only depends on the amount of iron in the sample, but also how this is distributed among the independent fluctuators[26]. In the considered frequency range of the experiments, the amplitude of the fluctuations increases with decreasing temperature. The simulations in Fig. 5 (b) and (e) show however that the different PSDs cross at higher frequencies, and that the total fluctuation amplitude will be conserved - as expected for Brownian fluctuations by Eq. 7.

We would further like to stress the magnitude of the influence of temperature on the fluctuations. Fig. 5 (c) and (f) show the noise power at 8 Hz of FCT and Perimag. In this 25 K interval, the noise power at 8 Hz decreases monotonously, and halves in amplitude.

In conclusion, the effect of temperature variations on fluctuations in MNP systems can be estimated with the presented model, which incorporates both the effect on the fluctuation timescale and the fluctuation amplitude. A general upper limit for the model is the Curie temperature of the magnetic core of the MNPs, above which they lose their magnetic properties. A lower limit on the Brownian fluctuations is the freezing point of the suspension. There is no real lower limit for the Néel fluctuations, since there is always a finite chance for the moment to switch against the anisotropy. However, realistically, below the blocking temperature, switching events of the moments become rare. Therefore, measurements of such fluctuations and their statistical analysis via the PSD become unfeasible. Although seldomly observed in MNP systems[27], quantum fluctuations between the energy minima set by the anisotropy of the particles form another switching mechanism that could contribute at lower temperatures.

The Néel fluctuation amplitude depends on temperature, and the trend depends on the considered field component and the geometry of the experiment. Counter-intuitively, the amplitude for the switching of the moment along the anisotropy axis decreases with increasing temperature. For randomly distributed anisotropy axes, the fluctuation amplitude is constant.

For Brownian fluctuations, the noise amplitude is independent of temperature and the timescales vary only slightly. However, even in a temperature range of 25 K, a distinctive difference in the PSDs of two MNP systems is found for biomedically relevant temperatures.

The presented findings are interesting from a fundamental point of view, since temperature is inextricably related to thermal noise. They help understanding all aspects of the noise signal of MNPs: the fluctuation timescales, the total noise amplitude, the power density at specific frequency ranges, and how they are coupled in the PSD. These results are thus important for noise related applications of MNP systems, e.g. the MNP characterization technique Thermal Noise Magnetometry[8]. Johnson Noise Thermometry[28] of electrical noise is also an inspiring example for noise based applications in MNP systems. Through magnetic noise measurements, MNPs could be used as nanothermometer for noninvasive local temperature measurements of the particles' microenvironment. The absence of an external probing field

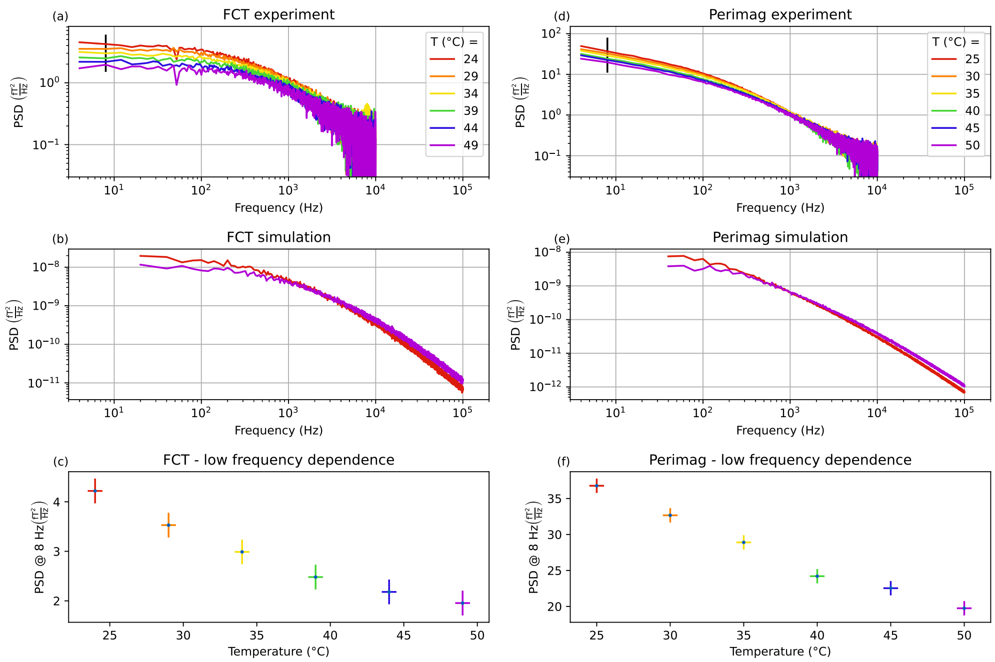

FIG. 5. Experimental PSDs of FCT and Perimag at different biomedically relevant temperatures (a,d). A lognormal size distribution is fitted to the PSDs at the lowest temperatures (24C (297.15 K) and 25C (298.15 K) and subsequently used as input for the simulations (b,e). The noise amplitude at 8 Hz for the experiments is plotted in panels (c,f).

- which potentially heats up the particles through hysteresis losses and consequently induces a local temperature rise - is a big advantage in this regard. Additionally, in-field immobilized MNPs are extra sensitive to temperature variations, since both the fluctuation amplitude and fluctuation timescale of MNPs with aligned anisotropy axes are depending on temperature. The power density of the thermal noise in a fixed frequency range of such a MNP system could be used as a sensitive and stable temperature measure.

SUPPLEMENTARY MATERIAL

Details about the simulations and the fitting to the experimental data can be found in the supplementary material. Also the analytical expressions and extra calculations on the moments of the secondary stochastic variable are provided.

ACKNOWLEDGMENTS

This work was supported by the German Research Foundation (DFG) through the Project "MagNoise: Establishing Thermal Noise Magnetometry for Magnetic Nanoparticle Characterization" under Grant FKZ WI4230/3-1. J. L. was supported by the Fonds Wetenschappelijk Onderzoek (FWO-Vlaanderen) with senior postdoctoral research fellowship No. 12W7622N. Part of the computational resources and services used in this work were provided by the VSC (Flemish Supercomputer Center), funded by Ghent University, the Research Foundation Flanders (FWO) and the Flemish Government – department EWI.

DATA AVAILABILITY STATEMENT

The data that support the findings of this study are available upon reasonable request.

[1] W. F. Brown, "Thermal Fluctuations of a Single-Domain Particle," Physical review **130**, 1677–1686 (1963).
[2] N. Smith and P. Arnett, "White-noise magnetization fluctuations in magnetoresistive heads," Appl. Phys. Lett **78**, 1448 (2001).

[3]B. Parks, M. Bapna, J. Igbokwe, H. Almasi, W. Wang, and S. A. Majetich, "Superparamagnetic perpendicular magnetic tunnel junctions for true random number generators," AIP Advances **8**, 55903 (2018).
[4]W. A. Borders, A. Z. Pervaiz, S. Fukami, K. Y. Camsari, H. Ohno, and S. Datta, "Integer factorization using stochastic magnetic tunnel junctions," Nature **573**, 390–393 (2019).
[5]N. Stutzke, S. L. Burkett, and S. E. Russek, "Temperature and field dependence of high-frequency magnetic noise in spin valve devices ARTICLES," Appl. Phys. Lett **82**, 91 (2003).
[6]R. Dusad, F. K. Kirschner, J. C. Hoke, B. R. Roberts, A. Eyal, F. Flicker, G. M. Luke, S. J. Blundell, and J. C. Davis, "Magnetic monopole noise," Nature **571**, 234–239 (2019), arXiv:1901.10044.
[7]M. Goryca, X. Zhang, J. Li, A. L. Balk, J. D. Watts, C. Leighton, C. Nisoli, P. Schiffer, and S. A. Crooker, "Field-Induced Magnetic Monopole Plasma in Artificial Spin Ice," Physical Review X **11**, 011042 (2021).
[8]J. Leliaert, A. Coene, M. Liebl, D. Eberbeck, U. Steinhoff, F. Wiekhorst, B. Fischer, L. Dupré, and B. Van Waeyenberge, "Thermal magnetic noise spectra of nanoparticle ensembles," Applied Physics Letters **107**, 222401 (2015).
[9]A. Einstein, "Über die von der molekularkinetischen Theorie der Wärme geforderte Bewegung von in ruhenden Flüssigkeiten suspendierten Teilchen," Annalen der Physik **322**, 549–560 (1905).
[10]Q. A. Pankhurst, T. K. Thanh, S. K. Jones, and J. Dobson, "Progress in applications of magnetic nanoparticles in biomedicine," Journal of Physics D: Applied Physics **42**, 15 (2009).
[11]T. K. Thanh, *Clinical Applications of Magnetic Nanoparticles* (CRC Press, 2018).
[12]A. Coene and J. Leliaert, "Magnetic nanoparticles in theranostic applications," Journal of Applied Physics **131**, 160902 (2022).
[13]R. Kubo, "The fluctuation-dissipation theorem," Reports on Progress in Physics **29**, 255 (1966).
[14]M. Alba, J. Hammann, M. Ocio, P. Refregier, and H. Bouchiat, "Spin-glass dynamics from magnetic noise, relaxation, and susceptibility measurements," Journal of Applied Physics **61**, 3683 (1987).
[15]S. A. A. Majetich and M. Sachan, "Magnetostatic interactions in magnetic nanoparticle assemblies: energy, time and length scales," Journal of Physics D: Applied Physics **39**, 407–422 (2006).
[16]G. Gomide, R. Cabreira Gomes, M. Gomes Viana, A. F. Cortez Campos, R. Aquino, A. López-Ortega, R. Perzynski, and J. Depeyrot, "Nanoparticle Size Distribution and Surface Effects on the Thermal Dependence of Magnetic Anisotropy," Journal of Physical Chemistry C **126**, 1581–1589 (2022).
[17]R. Soucaille, M. E. Sharifabad, and N. D. Telling, "Broadband optical measurement of AC magnetic susceptibility of magnetite nanoparticles," Applied Physics Letters **116**, 62404 (2020).
[18]S. Adhikari, Y. Wang, P. Spaeth, F. Scalerandi, W. Albrecht, J. Liu, and M. Orrit, "Magnetization Switching of Single Magnetite Nanoparticles Monitored Optically," arXiv preprint **arXiv:2207** (2022).
[19]P. Debye, *Polar Molecules* (Chemical Catalog Company, New York, 1929).
[20]N. Wiener, "Generalized harmonic analysis," Acta Mathematica **55**, 117–258 (1930).
[21]A. Khintchine, "Korrelationstheorie der stationären stochastischen Prozesse," Mathematische Annalen **109**, 604–615 (1934).
[22]The magnetic field $\mathbb{B}$ was calculated at a distance of 0.1 mm from a single macrospin with material parameters of magnetite ($K = 10$ kJ/m^3 and $M_S = 400$ kA/m) and water (η = 0.1 mPas). The moment was fluctuating purely under the Brownian or Néel mechanism. For the Brownian fluctuations, the diameter was chosen 40 nm; for the Néel fluctuations 20 nm.
[23]P. Svedlindh, T. Jonsson, and J. L. García-Palacios, "Intra-potential-well contribution to the AC susceptibility of a noninteracting nano-sized magnetic particle system," Journal of Magnetism and Magnetic Materials **169**, 323–334 (1997).
[24]F. Ludwig, C. Balceris, and C. Johansson, "The Anisotropy of the AC Susceptibility of Immobilized Magnetic Nanoparticles - the Influence of Intra-Potential-Well Contribution on the AC Susceptibility Spectrum," IEEE Transactions on Magnetics **53** (2017), 10.1109/TMAG.2017.2692038.
[25]R. Ackermann, F. Wiekhorst, A. Beck, D. Gutkelch, F. Ruede, A. Schnabel, U. Steinhoff, D. Drung, J. Beyer, C. Aßmann, L. Trahms, H. Koch, T. Schurig, R. Fischer, M. Bader, H. Ogata, and H. Kado, "Multichannel SQUID system with integrated magnetic shielding for magnetocardiography of mice," IEEE Transactions on Applied Superconductivity **17**, 827–830 (2007).
[26]K. Everaert, M. Liebl, D. Gutkelch, J. Wells, B. Van Waeyenberge, F. Wiekhorst, and J. Leliaert, "Noise power properties of magnetic nanoparticles as measured in Thermal Noise Magnetometry," IEEE Access **9**, 111505 (2021).
[27]W. Wernsdorfer, E. B. Orozco, K. Hasselbach, A. Benoit, D. Mailly, O. Kubo, H. Nakano, and B. Barbara, "Macroscopic Quantum Tunneling of Magnetization of Single Ferrimagnetic Nanoparticles of Barium Ferrite," Physics Letters **79**, 4014–4017 (1997).
[28]K. C. Jifeng Qu, Samuel P Benz, K. Z. , Horst Rogalla, Weston L Tew, Rod White, and Z. Zhou, "An improved electronic determination of the Boltzmann constant by Johnson noise thermometry," Metrologia **54**, 549–558 (2017).

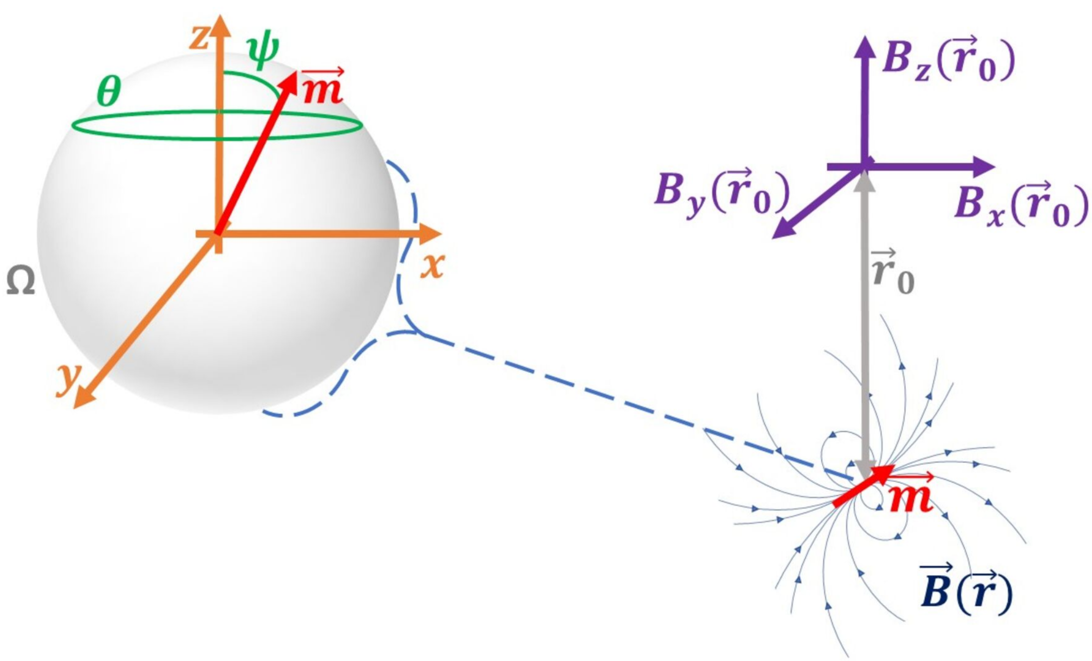
z
ψ
θ
$\vec{m}$
Ω
x
y
$B_z(\vec{r}_0)$
$B_y(\vec{r}_0)$
$B_x(\vec{r}_0)$
$\vec{r}_0$
$\vec{m}$
$\vec{B}(\vec{r})$

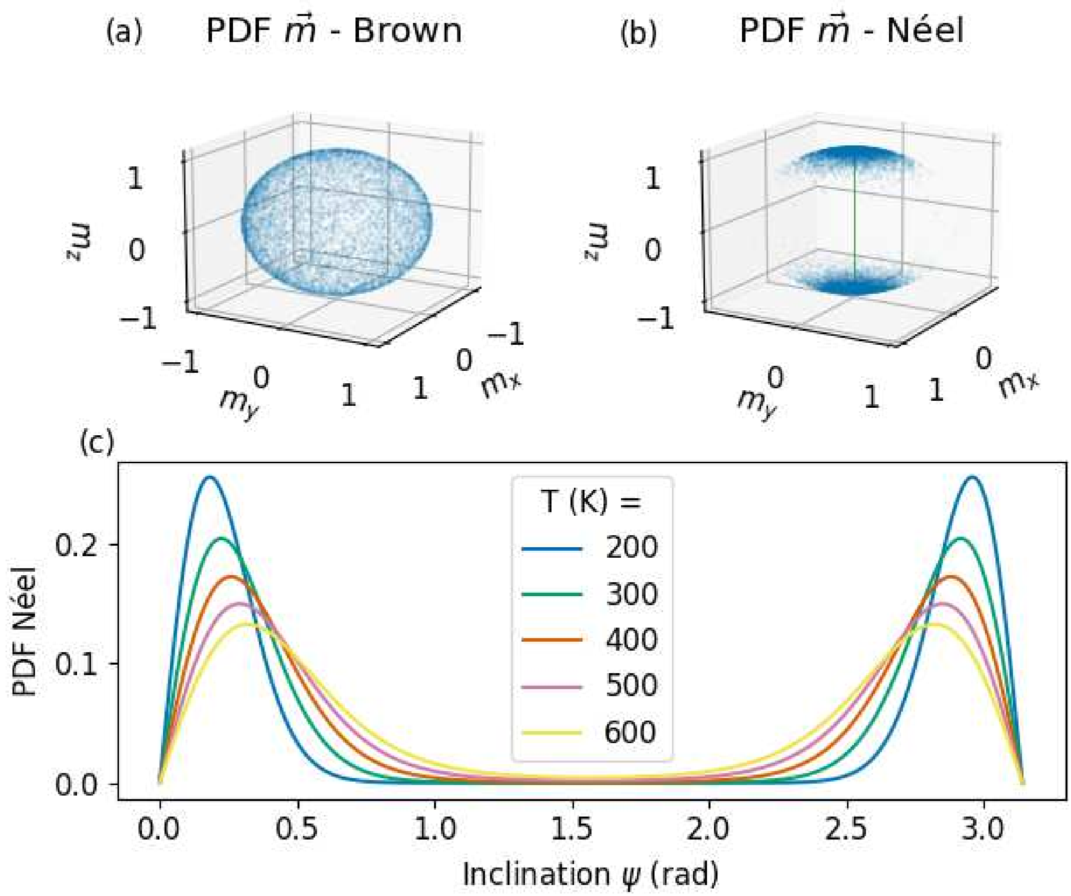
(a)
PDF $\vec{m}$ - Brown
(b)
PDF $\vec{m}$ - Néel
m_z
m_y
m_x
(c)
PDF Néel
Inclination ψ (rad)
T (K) =
200
300
400
500
600

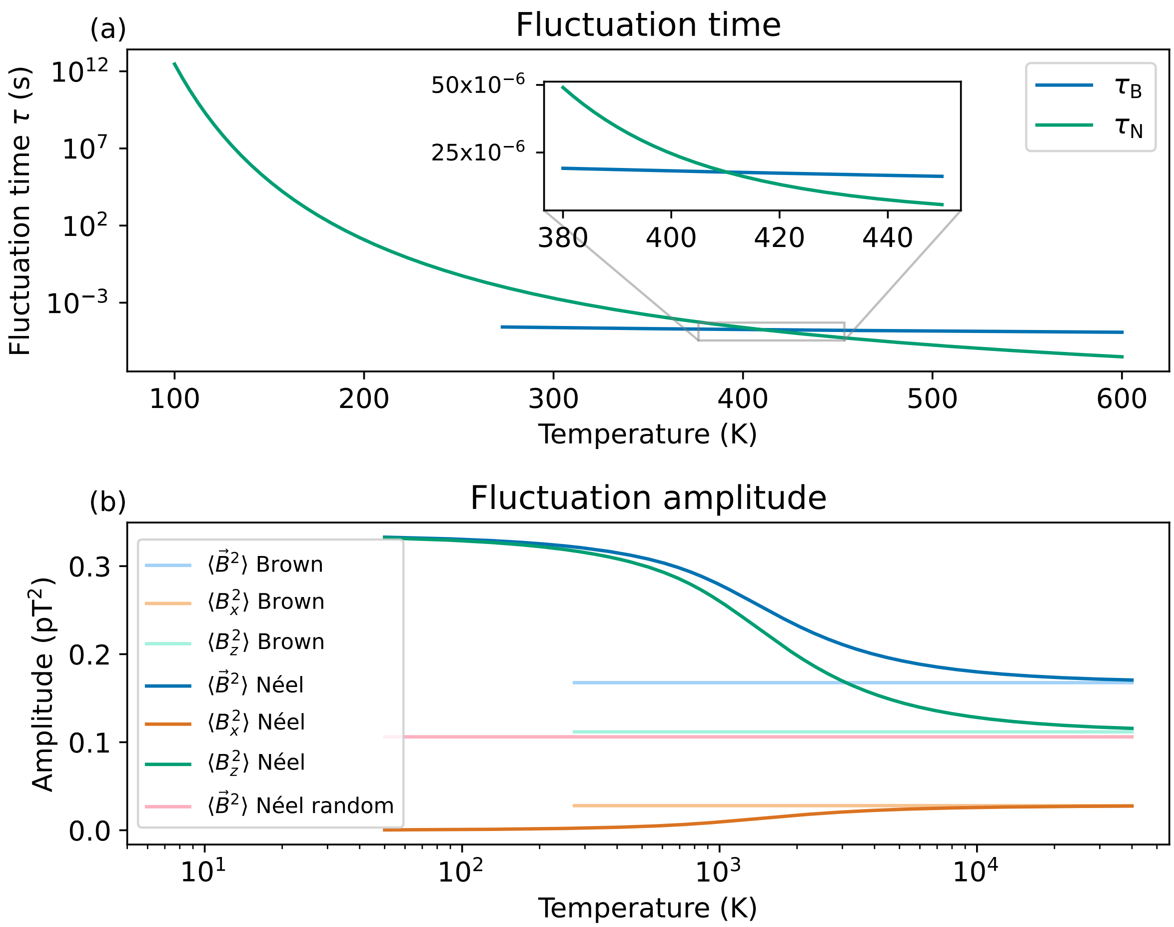
(a)
Fluctuation time
Fluctuation time τ (s)
10^{12}
10^{7}
10^{2}
10^{-3}
100
200
300
400
500
600
Temperature (K)
$50\mathrm{x}10^{-6}$
$25\mathrm{x}10^{-6}$
380
400
420
440
τ_B
τ_N
(b)
Fluctuation amplitude
Amplitude (pT^2)
0.3
0.2
0.1
0.0
10^1
10^2
10^3
10^4
Temperature (K)
$\langle \vec{B}^2 \rangle$ Brown
$\langle B_x^2 \rangle$ Brown
$\langle B_z^2 \rangle$ Brown
$\langle \vec{B}^2 \rangle$ Néel
$\langle B_x^2 \rangle$ Néel
$\langle B_z^2 \rangle$ Néel
$\langle \vec{B}^2 \rangle$ Néel random

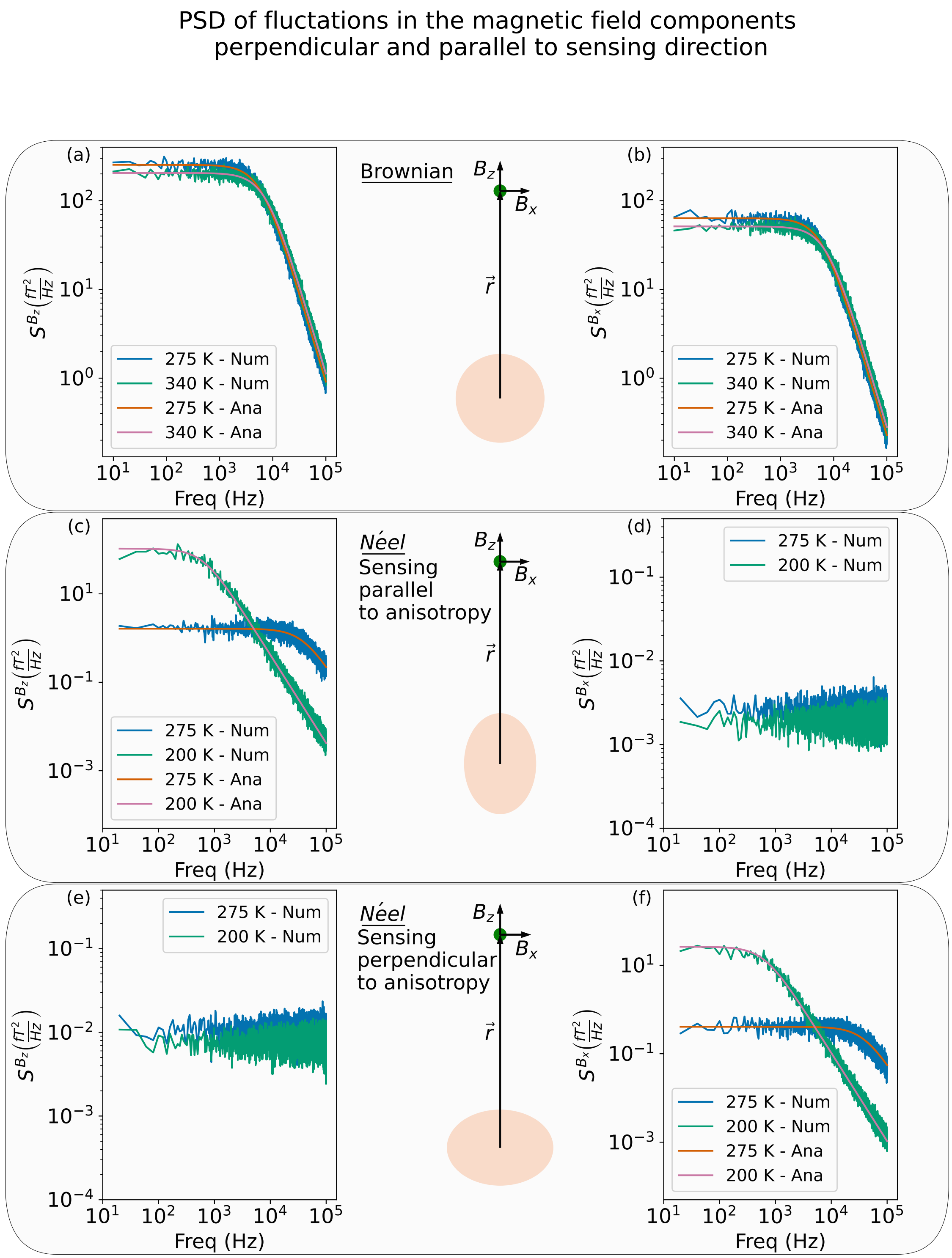
PSD of fluctations in the magnetic field components
perpendicular and parallel to sensing direction
(a)
(b)
Brownian
Néel
Sensing
parallel
to anisotropy
(c)
(d)
Néel
Sensing
perpendicular
to anisotropy
(e)
(f)
275 K - Num
340 K - Num
275 K - Ana
340 K - Ana
200 K - Num
200 K - Ana
Freq (Hz)

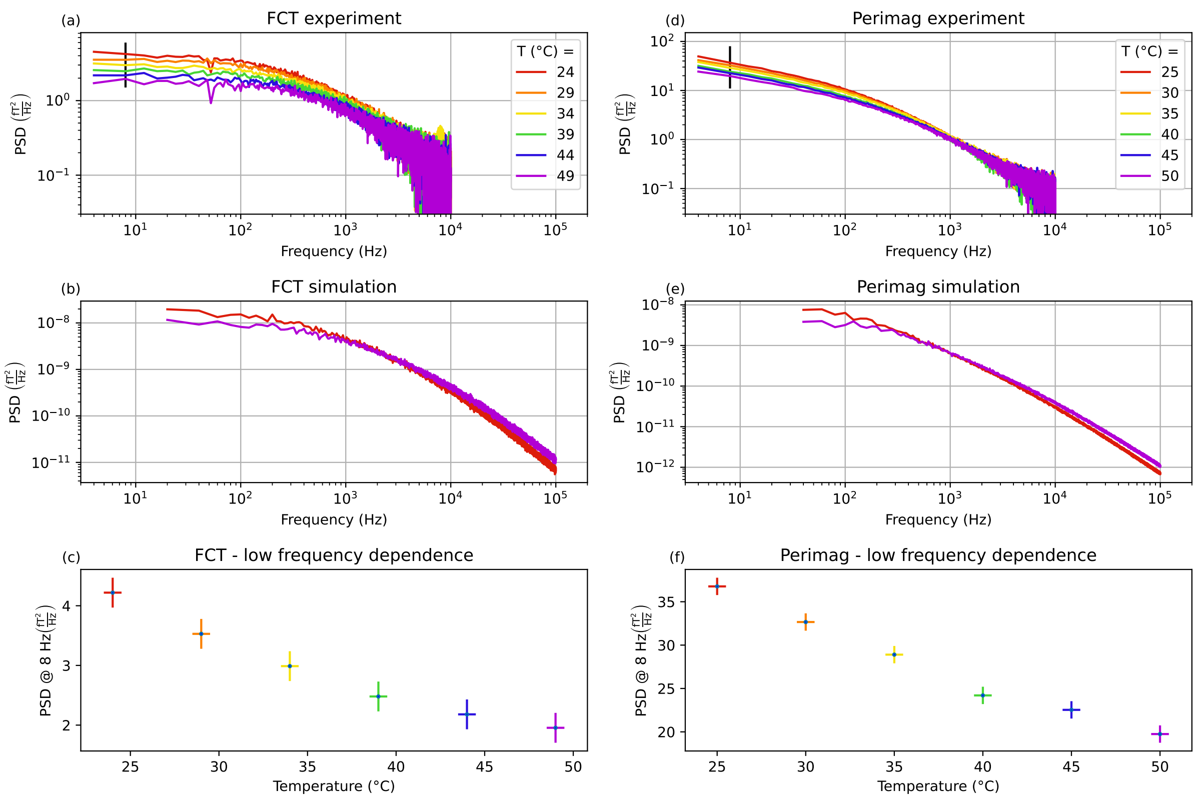
(a)
FCT experiment
T (°C) =
24
29
34
39
44
49
PSD
Frequency (Hz)
(d)
Perimag experiment
T (°C) =
25
30
35
40
45
50
PSD
Frequency (Hz)
(b)
FCT simulation
PSD
Frequency (Hz)
(e)
Perimag simulation
PSD
Frequency (Hz)
(c)
FCT - low frequency dependence
PSD @ 8 Hz
Temperature (°C)
(f)
Perimag - low frequency dependence
PSD @ 8 Hz
Temperature (°C)